Optics Letters

Quantum scattering theory of a single-photon Fock state in three-dimensional spaces

JINGFENG LIU,[1,2] MING ZHOU,[2] AND ZONGFU YU[2,*]

[1]College of Electronic Engineering, South China Agricultural University, Guangzhou 510642, China
[2]Department of Electrical and Computer Engineering, University of Wisconsin, Madison, Wisconsin 53706, USA
*Corresponding author: zyu54@wisc.edu

Received 3 June 2016; revised 14 July 2016; accepted 15 August 2016; posted 16 August 2016 (Doc. ID 267662); published 7 September 2016

A quantum scattering theory is developed for Fock states scattered by two-level systems in three-dimensional free space. It is built upon the one-dimensional scattering theory developed in waveguide quantum electrodynamics. The theory fully quantizes the incident light as Fock states and uses a non-perturbative method to calculate the scattering matrix.

OCIS codes: (270.0270) Quantum optics; (290.0290) Scattering.

http://dx.doi.org/10.1364/OL.41.004166

We develop a theory to solve the quantum scattering problem of Fock states in three-dimensional (3D) free spaces. It can solve the scattering problem of Fock-state light in the presence of any number of two-level systems (TLSs) in arbitrary spatial configurations. Our work is inspired by recent development in waveguide quantum electrodynamics (QED) [1–13]. Compared to approximated theories that treat the incident light as semi-classical fields, methods developed in [1–3] treat the incident field explicitly as Fock states and use a non-perturbative method to solve the scattering problem. As a result, they not only provide exact solutions, but also can solve multi-photon problems [4,8,11,14–25]. However, these methods [1–5,7–9,17,18,20,26,27] only apply to a one-dimensional (1D) space, such as a waveguide. Here, we extend the existing 1D theory to the 3D free space. Although we illustrate our theory based on single photons, the framework is compatible with multi-photon problems.

We start with a single TLS and then discuss the case of multiple TLSs in free space. The Hamiltonian for a TLS in free space has a rather simple form:

$$H = \hbar\omega_e \sigma^\dagger \sigma + \sum_k \hbar\omega_k a_k^\dagger a_k + \sum_k i\hbar g_k (a_k^\dagger \sigma - a_k \sigma^\dagger). \quad \textbf{(1)}$$

The first and the second terms are the free Hamiltonian of a TLS and free-space photons, respectively. The third term describes the interaction between them under the dipole and rotating-wave approximations. Here, $\hbar$ is a reduced Planck constant, and $i = \sqrt{-1}$. ω_e is the transition frequency of the TLS. $\sigma^\dagger$ and σ are the raising and lowering operator, respectively. $\omega_{\boldsymbol{k}}$ and $\mathbf{k}$ are the angular frequency and the wavevector of photons, respectively. $a_{\boldsymbol{k}}^\dagger$ and $a_{\boldsymbol{k}}$ are the bosonic creation and annihilation operator of the photons, respectively. The coupling coefficient is $g_{\boldsymbol{k}} = \boldsymbol{d} \cdot \boldsymbol{e}_{\boldsymbol{k}} \sqrt{\frac{\omega_e}{2\hbar\varepsilon_0 L^3}}$, where the transition dipole moment is $\boldsymbol{d}$, and $\boldsymbol{e}_k$ is the polarization of the light. L^3 is the normalization volume.

Our strategy is to convert the 3D problem to a form that allows us to apply the method in a 1D waveguide QED. We consider the 3D continuum as many *channels*, or "waveguides." Each channel represents a plane wave with a distinct direction. The light-TLS interaction in a channel can be treated as a waveguide QED problem, which has been successfully solved [1–3].

To implement the above strategy, we start by first discretizing the 3D continuum. It is realized by using a periodic boundary condition in the x–y plane [Fig. 1(a)]. The period is L. At the end of the derivation, we will take the limit of $L \to \infty$ to remove the effect of this boundary condition. Because of the periodicity, a normally incident photon can only be scattered to a set of discrete directions. These directions are defined by the waves' in-plane wavevectors $\boldsymbol{k}_{xy} = (m_x, m_y)2\pi/L$, where $m_{x,y}$ are integers [Fig. 1(b)]. We define these directions as channels. As a convention of the notation, the channel (m_x, m_y) in the upper semi-infinite space also includes the waves in lower semi-infinite space in the direction of $(-m_x, -m_y)2\pi/L$. Channels are all located within the circle of $k_e = \omega_e/c$ for the interested frequency range around the resonant frequency ω_e. The total number of channels is $N = \pi\lfloor L/\lambda_e\rfloor^2$, where $\lambda_e = 2\pi/k_e$ is the resonant wavelength. The floor operator $\lfloor A\rfloor$ gives the largest integer smaller than A. There are also two propagation directions in each channel, which are labeled with subscripts f (forward) and b (backward). There are also two polarizations in each channel. Using channels, we can convert the Hamiltonian to

$$\begin{aligned} H = {} & \hbar\omega_e \sigma^\dagger \sigma + \sum_{n=1}^{N} \sum_k \hbar\omega_{k,n} (a_{k,n_f}^\dagger a_{k,n_f} + a_{k,n_b}^\dagger a_{k,n_b}) \\ & + \sum_{n=1}^{N} \sum_k i\hbar \mathbb{N}(\theta_n, \varphi_n) g_k [(a_{k,n_f}^\dagger + a_{k,nb}^\dagger)\sigma \\ & - (a_{k,n_f} + a_{k,n_b})\sigma^\dagger]. \end{aligned} \quad \textbf{(2)}$$

It is important to note that the wavenumber k is a scalar now because the information of the propagation direction is

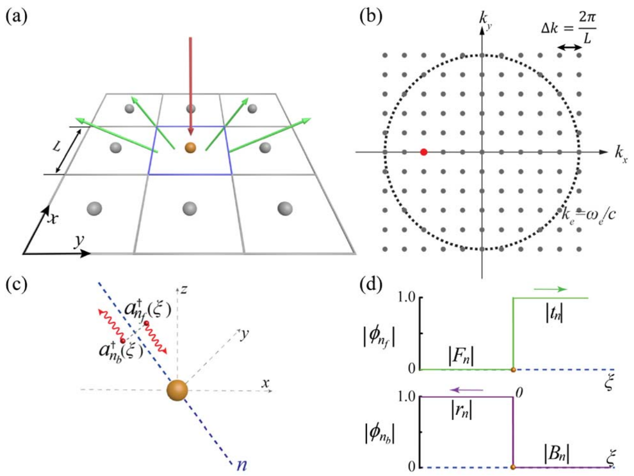

Fig. 1. (a) Periodic boundary conditions are set up for the derivation purpose. A single TLS is in the free space. The period is L. We take $L \to \infty$ at the end of the derivation. (b) Distribution of channels in the k-space. Due to the periodicity, the scattered light has discrete wavevectors in the k_{xy}-plane, represented by dots. (c) Spatial operator $a^\dagger_{n_{f/b}}(\xi)$ creates a forward or backward moving photon at the location ξ in the nth channel. (d) Schematic of the magnitude of the spatial wavefunction $|\phi_{n_{f/b}}(\xi)|$ for the forward (green line) and backward (purple line) directions in the nth channel.

absorbed into the channel definition. Because of the periodic boundary condition, we need to normalize the coupling coefficient with a factor $\mathbb{N}(\theta_n, \varphi_n) = \sqrt{(\cos^2\varphi_n - \sin^2\varphi_n)/\cos\theta_n}$, where θ_n and φ_n are the polar and azimuthal angles of the nth channel, respectively [28,29].

To solve for the spatial wavefunctions, we further convert the Hamiltonian to a real-space representation by applying the following Fourier transformation:

$$a^\dagger_{k,n_{f/b}} = \frac{1}{\sqrt{L}} \int_{-\infty}^{\infty} \mathrm{d}\xi a^\dagger_{n_{f/b}}(\xi) \exp(ik\xi), \tag{3a}$$

$$a_{k,n_{f/b}} = \frac{1}{\sqrt{L}} \int_{-\infty}^{\infty} \mathrm{d}\xi a_{n_{f/b}}(\xi) \exp(-ik\xi), \tag{3b}$$

where ξ is the spatial coordinate alone the nth channel, as shown in Fig. 1(c). The operator $a^\dagger_{n_{f/b}}(\xi)$ creates a forward or backward moving photon at location ξ in the nth channel. This transformation has been used for the scattering theory in a 1-D continuum, such as waveguide QED [2,3]. Substituting Eq. (3) into Eq. (2), we get the real-space Hamiltonian

$$\begin{aligned} H = \hbar\omega_e\sigma^\dagger\sigma + \sum_{n=1}^{N} \int_{-\infty}^{+\infty} \mathrm{d}\xi \Big\{ \Big[(-i\hbar c) a^\dagger_{n_f}(\xi) \frac{d}{d\xi} a_{nf}(\xi) \\ + (i\hbar c) a^\dagger_{n_b}(\xi) \frac{d}{d\xi} a_{nb}(\xi) \Big] \\ + i\hbar g_n \delta(\xi) [[a^\dagger_{nf}(\xi) + a^\dagger_{n_b}(\xi)]\sigma - [a_{nf}(\xi) + a_{nb}(\xi)]\sigma^\dagger] \Big\}, \end{aligned} \tag{4}$$

where c is the speed of light, and $g_n = \sqrt{L(\cos^2\varphi_n - \sin^2\varphi_n)/\cos\theta_n} g_k$. $\delta(\xi)$ is the Dirac delta function.

For a single photon, the eigenstate of the Hamiltonian in Eq. (4) can be written as

$$|\phi\rangle = \left(\sum_{n=1}^{N} \int \mathrm{d}\xi (\phi_{n_f}(\xi) a^\dagger_{n_f}(\xi) + \phi_{n_b}(\xi) a^\dagger_{n_b}(\xi)) + e\sigma^\dagger \right) |0, g\rangle, \tag{5}$$

where $|0, g\rangle$ represents the ground state. e is the probability amplitude of the TLS in the excited state; $\phi_{n_{f/b}}(\xi)$ are the spatial distributions of the amplitudes in the channels. We can now directly evaluate e and $\phi_{n_{f/b}}(\xi)$ using the time-independent Schrödinger equation $H|\phi\rangle = \hbar\omega|\phi\rangle$ and obtain

$$-ic \frac{d}{d\xi} \phi_{n_f}(\xi) + i g_n \delta(\xi) e = \omega \phi_{n_f}(\xi), \tag{6a}$$

$$ic \frac{d}{d\xi} \phi_{n_b}(\xi) + i g_n \delta(\xi) e = \omega \phi_{n_b}(\xi), \tag{6b}$$

$$\omega_e e - i \sum_{n=1}^{N} g_n (\phi_{n_f}(0) + \phi_{n_b}(0)) = \omega e. \tag{6c}$$

These linear differential equations can be easily solved. Specifically, Eq. (6a) reduces to $-ic \frac{d}{d\xi} \phi_{n_f}(\xi) = \omega \phi_{n_f}(\xi)$ for $\xi \neq 0$, which has a simple solution:

$$\phi_{n_f}(\xi) = F_n e^{ik\xi} \theta(-\xi) + t_n e^{ik\xi} \theta(\xi), \tag{7a}$$

where the wave number $k = \omega/c$. Similarly, for the backward directions, Eq. (6b) leads to

$$\phi_{n_b}(\xi) = r_n e^{-ik\xi} \theta(-\xi) + B_n e^{-ik\xi} \theta(\xi). \tag{7b}$$

In a scattering process, coefficients F_n and B_n can be interpreted as the incident amplitudes of the photon in the forward and backward directions, respectively. t_n and r_n represent the transmitted amplitudes in the forward and backward directions, respectively. These coefficients must satisfy the boundary condition at the location of the TLS: $F_n + t_n = r_n + B_n$. The boundary conditions at infinity are determined by the incident condition.

Now we consider a single-photon incident in the lth channel in the forward direction. Then we have $F_n = \delta_{nl}$ and $B_n = 0$. The wavefunctions $|\phi_{n_{f/b}}(\xi)|$ are schematically shown in Fig. 1(d) for a channel $n \neq l$. The forward and backward scattering amplitudes are represented by t_n and r_n, respectively. Using Eqs. (6) and (7), we can calculate these coefficients as

$$t_n = \frac{-i g_n g_l / c}{(\omega - \omega_e) + i\Gamma_0/2} + \delta_{nl}, \tag{8a}$$

$$r_n = \frac{-i g_n g_l / c}{(\omega - \omega_e) + i\Gamma_0/2}, \tag{8b}$$

$$e = \frac{-i g_l}{(\omega - \omega_e) + i\Gamma_0/2}, \tag{9}$$

where $\Gamma_0 = d^2\omega_e^3/(3\pi\hbar\varepsilon_0 c^3)$ is the spontaneous emission rate of the TLS in free space.

Now we have the complete spatial wavefunction of the eigenstates, from which we can obtain all the characteristics of the scattering process. We will briefly discuss a few examples below, although the results can also be obtained using many existing theories for this simple case.

The spatial distribution of the scattered photon can be directly evaluated by summing the amplitudes in all channels $\phi_p(r) = \sum_{n=1}^{N}[\phi_{n_f}(\xi_n) + \phi_{n_b}(\xi_n)]$. ξ_n is calculated by projecting the position $\boldsymbol{r}$ onto the nth channels. Specifically, we consider a TLS with a dipole moment induced by a linearly polarized incident light. The incident photon propagates along the z axis and is polarized alone the x direction [into the plane in Fig. 2(a)]. Figure 2(a) shows the real part of the scattering wavefunction $\phi_p(r)$ in the xy plane. It clearly shows a dipole radiation profile.

We can also easily calculate the differential and total cross sections. For example, the total scattering cross section [30] is

$$\sigma(\omega) = \frac{\sum_{n=1}^{N}(t_n^\dagger)t_n + \sum_{n=1}^{N}(r_n^\dagger)r_n}{1/L^2}. \quad \textbf{(10)}$$

Substituting r_n and t_n into Eq. (10), we obtain

$$\sigma(\omega) = \frac{3\lambda_e^2}{2\pi}\frac{(\Gamma_0/2)^2}{(\omega - \omega_e)^2 + (\Gamma_0/2)^2}. \quad \textbf{(11)}$$

The cross-sectional spectrum is shown in Fig. 2(b), which shows the typical Lorentzian lineshape with a bandwidth defined by the spontaneous emission rate Γ_0.

The complete wavefunction also allows us to calculate the group delay $\tau = d\varphi/d\omega$ for the photon when scattered by a TLS. The scattering phase φ can be directly evaluated from the wavefunction as $\varphi(\omega) = \arctan\{-\Gamma_0/[2(\omega - \omega_e)]\}$, which leads to a Winger time delay $\tau = \frac{\Gamma_0/2}{(\omega-\omega_e)^2+(\Gamma_0/2)^2}$.

All these results confirm the calculation based on semi-classical scattering theories [31–33]. Below, we further show that the theory easily accommodates multiple TLSs. Specifically, we use two TLSs as an example to illustrate the method. The Hamiltonian can be written as

$$H = \sum_{m=1}^{2}\hbar\omega_m\sigma_m^\dagger\sigma_m + \hbar\Omega_{12}(\sigma_1^\dagger\sigma_2 + \sigma_2^\dagger\sigma_1) + \sum_k \hbar\omega_k a_k^\dagger a_k + \sum_{m=1}^{2}\sum_k i\hbar g_{mk}(a_k^\dagger\sigma_m - a_k\sigma_m^\dagger), \quad \textbf{(12)}$$

where Ω_{12} is the strength of the dipole–dipole interaction between the two TLSs [34,35]. Following a similar procedure, we convert it to a real-space representation using the channels

$$\begin{aligned} H = {} & \sum_{m=1}^{2}\hbar\omega_m\sigma_m^\dagger\sigma_m + \hbar\Omega_{12}(\sigma_1^\dagger\sigma_2 + \sigma_2^\dagger\sigma_1) \\ & + \sum_{n=1}^{N}\int_{-\infty}^{\infty}\mathrm{d}\xi\left[(-i\hbar c)a_{n_f}^\dagger(\xi)\frac{d}{\mathrm{d}\xi}a_{nf}(\xi)\right. \\ & \left. + (i\hbar c)a_{n_b}^\dagger(\xi)\frac{d}{d\xi}a_{nb}(\xi)\right] \\ & + i\hbar\sum_{n=1}^{N}\int_{-\infty}^{\infty}\mathrm{d}\xi\sum_{m=1}^{2}g_{n,m}\delta(\xi - \xi_{n,m})\{[a_{nf}^\dagger(\xi) \\ & + a_{n_b}^\dagger(\xi)]\sigma_m - [a_{nf}(\xi) + a_{nb}(\xi)]\sigma_m^\dagger\}, \end{aligned} \quad \textbf{(13)}$$

where $\xi_{n,m}$ is the projected location of the mth TLS in the nth channel. The general form of the eigenfunction for a single excitation can be written as

$$\begin{aligned} |\phi\rangle = {} & \sum_{n=1}^{N}\int \mathrm{d}\xi\{[\phi_{n_f}(\xi)a_{n_f}^\dagger(\xi) + \phi_{n_b}(\xi)a_{n_b}^\dagger(\xi)] + e_1\sigma_1^\dagger \\ & + e_2\sigma_2^\dagger\}|0, g_1, g_2\rangle, \end{aligned} \quad \textbf{(14)}$$

where $|0, g_1, g_2\rangle$ is the ground state.

The forward and backward wavefunctions have three distinct segments, as divided by two TLSs:

$$\begin{aligned} \phi_{n_f}(\xi) = {} & e^{ik\xi}[F_n\theta(\xi_{n,1} - \xi) + C_n\theta(\xi - \xi_{n,1})\theta(\xi_{n,2} - \xi) \\ & + t_n\theta(\xi - \xi_{n,2})], \end{aligned} \quad \textbf{(15a)}$$

$$\begin{aligned} \phi_{n_b}(\xi) = {} & e^{-ik\xi}[r_n\theta(\xi_{n,1} - \xi) + D_n\theta(\xi - \xi_{n,1})\theta(\xi_{n,2} - \xi) \\ & + B_n\theta(\xi - \xi_{n,2})]. \end{aligned} \quad \textbf{(15b)}$$

All the coefficients $F_n, C_n, t_n, r_n, D_n,$ and B_n can be obtained by solving the Schrödinger equation. They are also constrained by the boundary conditions at the locations of the two TLSs and at infinity.

Similar to the single TLS case, F_n and B_n represent the incident photon in the forward and backward directions, respectively. Except for the incident directions, as shown schematically in Fig. 3(b), $F_n = B_n = 0$ for all other channels. t_n and r_n are the amplitudes of the scattered photon in the forward and backward directions, respectively.

Different from the single TLS case, here we have additional terms: C_n and D_n. They are the amplitudes of the waves between the two TLSs. These waves induce the radiative interactions among the TLSs. They are responsible for

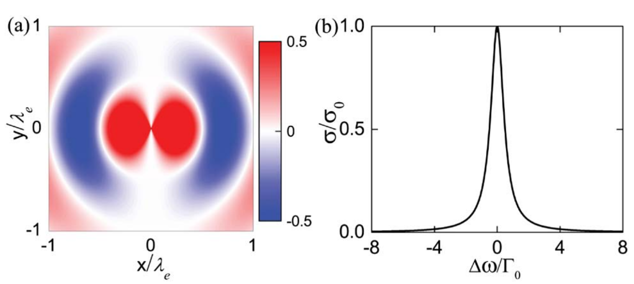

Fig. 2. (a) Snapshot of the real part of the scattered amplitude $\phi_p(\boldsymbol{r})$ for a single photon scattered by a TLS in the x–y plane where $z = 0$. The amplitude scales as $1/r$ with r being the distance to the TLS. (b) Spectrum of the scattering cross section.

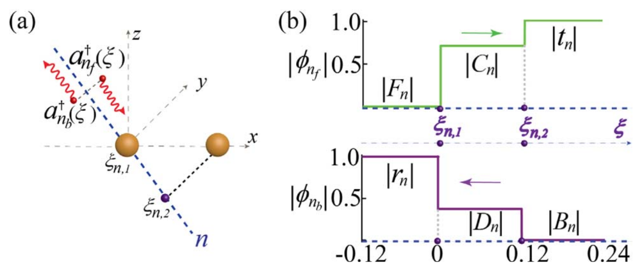

Fig. 3. (a) Schematic of a channel with two TLSs. The first TLS is located at the origin; thus, $\xi_{n,1} = 0$ for all channels. (b) Schematic of the magnitude of the photon wavefunction $|\phi_{n_{f/b}}(\xi)|$ for the forward (green line) and backward (purple line) directions in the nth channel. The distance between two TLSs is $0.15\lambda_e$.

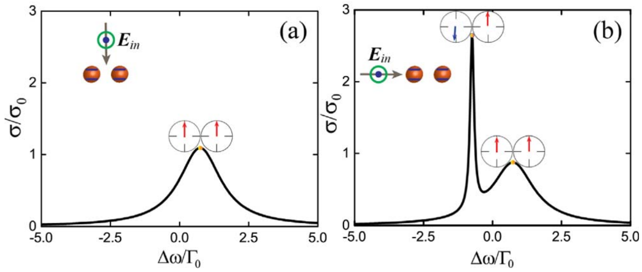

Fig. 4. Scattering cross section of the photon incident from (a) the normal direction and (b) the axial direction. The complex amplitudes of e_1 and e_2 of two TLSs are illustrated by vectors in a circle as shown in the insets. Two red arrows in (a) show that the two TLSs are in phase at the peak frequency. On the other hand, the sharp peaks in (b) exhibit the opposite phases for the amplitudes of the two TLSs.

collective effects, such as the superradiant spontaneous emission [36–40].

We now consider the specific example of a single photon scattered by two identical TLSs located at $x = 0$ and at $x = 0.15\lambda_e$ with λ_e being the resonant wavelength. The directions of their dipole moments are induced by the incident light.

Figure 4 shows the spectra of the cross section calculated from the quantum scattering theory. For a single-photon incident from the normal direction [Fig. 4(a)], the spectral bandwidth is $1.85\Gamma_0$, which is nearly double that in the case of the single TLS [Fig. 2(b)]. This bandwidth broadening is the manifest of the superradiance in the scattering process. The superradiance can be more clearly observed by examining the complex amplitudes e_1 and e_2 of the two TLSs, which are shown as the inset of Fig. 4(a). They show the same phase and amplitude.

When a single photon is incident in the axial direction [Fig. 4(b)], a second sharp peak appears in the spectrum of the cross section. The central frequency of the narrow peak is $\omega_e - 0.74\Gamma_0$. This peak is associated with the subradiant oscillation of the two TLSs. The excitation amplitudes of the two TLSs exhibit opposite phases, as shown by the inset of Fig. 4(b). The opposite-phase oscillation strongly reduces the radiation rate, resulting in an extremely narrow linewidth which reaches to $0.16\Gamma_0$. It also leads to a larger cross section $\sigma = 2.5\sigma_0$ which is larger than the linear addition for two TLSs, i.e., $2\sigma_0$. Since the two TLSs have opposite phases, this oscillation mode cannot be excited from the normal direction and, thus, is absent in the spectrum shown in Fig. 4(a).

In conclusion, we developed a quantum scattering theory for the quantum transport of Fock states in free space. We illustrated our theory using the simple case of one TLS in free space. The theory can accommodate any number of TLSs, which we illustrate using a case of two TLSs in free space.

Funding. National Science Foundation (NSF) (ECCS 1405201, ECCS 1641006); National Natural Science Foundation of China (NSFC) (11204089, 11334015, 11504115); China Scholarship Council (CSC).

Acknowledgment. J. Liu acknowledges the support from the CSC. M. Zhou achowledges the support of 3M fellowship.

REFERENCES

1. J. T. Shen and S. Fan, Opt. Lett. **30**, 2001 (2005).
2. J. T. Shen and S. Fan, Phys. Rev. A **79**, 023837 (2009).
3. H. Zheng, D. J. Gauthier, and H. U. Baranger, Phys. Rev. A **82**, 063816 (2010).
4. S. Fan, Ş. E. Kocabaş, and J. T. Shen, Phys. Rev. A **82**, 063821 (2010).
5. D. Witthaut and A. S. Sørensen, New J. Phys. **12**, 043052 (2010).
6. W. Chen, G. Y. Chen, and Y. N. Chen, Opt. Lett. **36**, 3602 (2011).
7. C. H. Yan, L. F. Wei, W. Z. Jia, and J. T. Shen, Phys. Rev. A **84**, 045801 (2011).
8. H. Zheng, D. J. Gauthier, and H. U. Baranger, Phys. Rev. A **85**, 043832 (2012).
9. H. Zheng and H. U. Baranger, Phys. Rev. Lett. **110**, 113601 (2013).
10. C. Gonzalez-Ballestero, E. Moreno, and F. J. Garcia-Vidal, Phys. Rev. A **89**, 042328 (2014).
11. N. Anders, K. Philip Trøst, P. S. M. Dara, K. Per, and M. Jesper, New J. Phys. **17**, 023030 (2015).
12. I. Söllner, S. Mahmoodian, S. L. Hansen, L. Midolo, A. Javadi, G. Kiršanskė, T. Pregnolato, H. El-Ella, E. H. Lee, J. D. Song, S. Stobbe, and P. Lodahl, Nat. Nano. **10**, 775 (2015).
13. F. Fratini, E. Mascarenhas, L. Safari, J. P. Poizat, D. Valente, A. Auffèves, D. Gerace, and M. F. Santos, Phys. Rev. Lett. **113**, 243601 (2014).
14. J. T. Shen and S. Fan, Phys. Rev. A **76**, 062709 (2007).
15. J. T. Shen and S. Fan, Phys. Rev. Lett. **98**, 153003 (2007).
16. P. Longo, P. Schmitteckert, and K. Busch, Phys. Rev. A **83**, 063828 (2011).
17. E. Rephaeli, Ş. E. Kocabaş, and S. Fan, Phys. Rev. A **84**, 063832 (2011).
18. D. Roy, Phys. Rev. Lett. **106**, 053601 (2011).
19. T. Shi, S. Fan, and C. P. Sun, Phys. Rev. A **84**, 063803 (2011).
20. H. Zheng, D. J. Gauthier, and H. U. Baranger, Phys. Rev. Lett. **107**, 223601 (2011).
21. T. Shi and S. Fan, Phys. Rev. A **87**, 063818 (2013).
22. T. Shi, D. E. Chang, and J. I. Cirac, Phys. Rev. A **92**, 053834 (2015).
23. S. Xu, E. Rephaeli, and S. Fan, Phys. Rev. Lett. **111**, 223602 (2013).
24. M. Laakso and M. Pletyukhov, Phys. Rev. Lett. **113**, 183601 (2014).
25. Ş. Ekin Kocabaş, Opt. Lett. **41**, 2533 (2016).
26. K. Lalumière, B. C. Sanders, A. F. van Loo, A. Fedorov, A. Wallraff, and A. Blais, Phys. Rev. A **88**, 043806 (2013).
27. H. Zheng, D. J. Gauthier, and H. U. Baranger, Phys. Rev. Lett. **111**, 090502 (2013).
28. L. Verslegers, Z. Yu, P. B. Catrysse, and S. Fan, J. Opt. Soc. Am. B **27**, 1947 (2010).
29. L. Verslegers, Z. Yu, Z. Ruan, P. B. Catrysse, and S. Fan, Phys. Rev. Lett. **108**, 083902 (2012).
30. M. Zhou, L. Shi, J. Zi, and Z. Yu, Phys. Rev. Lett. **115**, 023903 (2015).
31. E. P. Wigner, Phys. Rev. **98**, 145 (1955).
32. M. Pototschnig, Y. Chassagneux, J. Hwang, G. Zumofen, A. Renn, and V. Sandoghdar, Phys. Rev. Lett. **107**, 063001 (2011).
33. R. Bourgain, J. Pellegrino, S. Jennewein, Y. R. P. Sortais, and A. Browaeys, Opt. Lett. **38**, 1963 (2013).
34. S. Mokhlespour, J. E. M. Haverkort, G. Slepyan, S. Maksimenko, and A. Hoffmann, Phys. Rev. B **86**, 245322 (2012).
35. Z. Ficek and S. Swain, *Quantum Interference and Coherence: Theroy and Experiments* (Springer, 2005), Chaps. 2 and 3.
36. R. H. Dicke, Phys. Rev. **93**, 99 (1954).
37. R. G. DeVoe and R. G. Brewer, Phys. Rev. Lett. **76**, 2049 (1996).
38. A. Goban, C. L. Hung, J. D. Hood, S. P. Yu, J. A. Muniz, O. Painter, and H. J. Kimble, Phys. Rev. Lett. **115**, 063601 (2015).
39. D. W. Wang, R. B. Liu, S. Y. Zhu, and M. O. Scully, Phys. Rev. Lett. **114**, 043602 (2015).
40. M. Zhou, S. Yi, T. S. Luk, Q. Gan, S. Fan, and Z. Yu, Phys. Rev. B **92**, 024302 (2015).